The Optimization of Breathing Signals and Ventilatory Control with Nonlinear Respiratory Mechanics under Hypercapnia and Eucapnia

Shyan-Lung Lin[1*], Yu-Zhe Tsai[1], Andy Liao[2]

[1]Department of Automatic Control Engineering, Feng Chia University, Taichung, Taiwan
[2]Master's Program in Biomedical Informatics and Biomedical Engineering, Feng Chia University, Taichung, Taiwan

{sllin, m9887438, m0156250}@fcu.edu.tw

Abstract. In this study, the optimal human respiratory control model proposed earlier was modified to include the nonlinear respiratory mechanics by replacing the resistance with a lumped viscous resistance of the flow through total respiratory system, and a resistance of flow which is proportional to the power of flow rate. To evaluate the effect of the nonlinear respiratory mechanics in the optimal respiratory control, the model was simulated under hypercapnia and eucapnia with CO_2 inhalation and exercise input. The optimized breathing signals, including neuromuscular drive, airflow, and lung volume profiles, were demonstrated and the ventilatory responses with the optimized breathing patterns were examined. In comparison with the simulation result of linear respiratory mechanics, the nonlinear model was found to optimize the neuromuscular drive and airflow with ramplike and triangular waveform, respectively.

Keywords: Optimal respiratory control. Breathing signals. Nonlinear mechanics. CO_2 inhalation. Exercise.

1 Introduction

It has long been observed that the control of breathing pattern is consistent with the minimization of some measures of respiratory cost [1,2]. Among those respiratory control models developed lately [3-6], possible optimality principle has found to be existed in the modeling of the respiratory control [5,6]. Poon [5] suggested that the normal ventilatory responses to chemical stimuli, exercise inputs, and mechanical loadings are predicted by the minimization of a controller objective function that consists of the total chemical and mechanical costs of breathing. The hypothesis was later extended to model the integrative control of ventilatory responses and respiratory patterns, by expressing respiratory work rate of breathing in terms of the isometric respiratory driving pressure [7]. Based on the optimal respiratory control model [6,7], a simulation platform implemented under Matlab [8], was later revised using LabVIEW [9], to provide a real-time simulation tool for respiratory control, and a signal monitoring platform for instantaneous profiles and breathing pattern.

Previously we have demonstrated the optimized instantaneous respiratory profiles, ventilatory responses, and breathing patterns during CO_2 inhalation, eucapnic and hypercapnic exercises by using the optimal chemical-mechanical respiratory control model with several performance index to mimic the combined cost of breathing [7,8]. The effects of respiratory mechanical loadings (resistive and elastic)[9] and external dead space loading [10-11] on model behavior were also examined with experimental findings [12-16]. The mechanical effector system that related the neural respiratory output to the resultant mechanical airflow was described by the electrical RC model based on a lumped-parameter model proposed by Younes and Riddle [13,14]. A set of linear parameters R_{rs} and E_{rs} [7] were employed to represent the total flow-resistive and volume-elastic components, respectively. These include the passive resistance and elastance of the lung, chest wall, and airways.

Unfortunately, previous experimental or modeling studies on breathing mechanics can provide little information on how they affect the respiratory signals and breathing patterns simultaneously under any disturbances in the inhaled and metabolic production of CO_2. Recently, the needs for a simulation model of respiratory mechanics in biomedical education [17,18], clinical studies [19,20], and respiratory therapy of acute patients [21-22] have notably increased. In this paper, we extend an earlier model optimal respiratory control to replace the linear RC model with the nonlinear model respiratory mechanics employed by Hirayama et al. [5], instead of using an inspiratory sinusoidal airflow waveform, we employed a neuro-muscular driving pressure with quadratic function in the inspiratory phase and exponential discharge in the expiratory phase for optimization. The airflow and lung volume profiles will be optimized through a neural mechanical effector with the nonlinear model of respiratory mechanics and the comparative simulation was performed under eucapnia and hypercapnia.

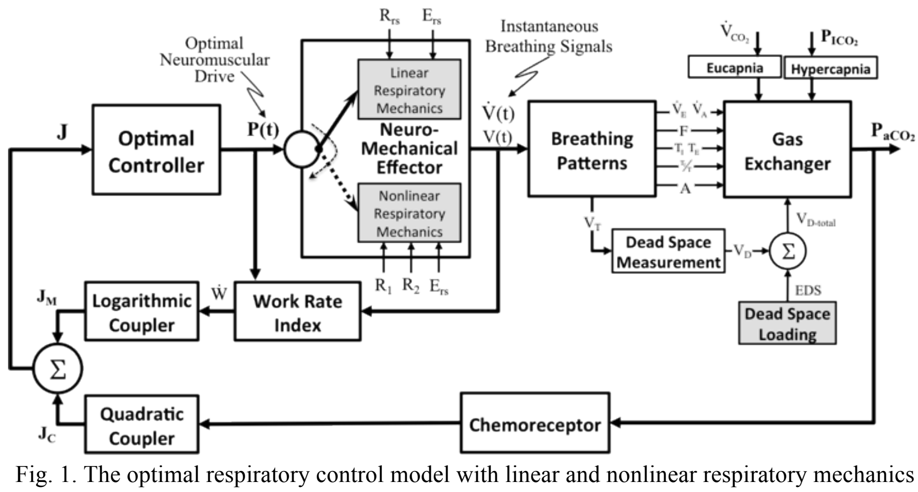

Fig. 1. The optimal respiratory control model with linear and nonlinear respiratory mechanics

2 The Optimal Respiratory Control

The model of the optimal chemical-mechanical respiratory control and simulation prospect of current study are illustrated in Fig. 1.

2.1 Optimization Indexes

The optimal controller in the model is driven by both chemical and neuro-mechanical feedback signals. In Fig. 1, this is demonstrated by the coupling of chemical cost (J_C) and mechanical cost (J_M), represented by the chemical feedback signal quadratic coupler and the work rate logarithmic coupler, respectively. The optimal control output is determined by the minimum of J. The mathematical descriptions of the optimization indexes have been detailed in earlier reports [8-10] and are outlined below in Eqs. (1)~(4):

$$J = J_C + J_M \ , \tag{1}$$

$$J_C = \alpha^2 \cdot \left(P_{aCO_2} - \beta\right)^2 \ , \tag{2}$$

$$J_M = \ln \dot{W} \ , \tag{3}$$

$$\begin{aligned} \dot{W} &= \dot{W}_I + \lambda \cdot \dot{W}_E \\ \dot{W}_I &= \frac{1}{T}\int_0^{T_I} \frac{P(t)\cdot\dot{V}(t)}{\xi_1^n \cdot \xi_2^n} dt \\ \dot{W}_E &= \frac{1}{T}\int_{T_I}^{T} P(t)\cdot\dot{V}(t)\, dt \end{aligned} \quad . \tag{4}$$

In Eq. (4), the total mechanical index is assumed to be a weighted sum of the inspiratory and expiratory indices, with a weighting parameter λ, and where $\dot{W}$, $\dot{W}_I$, $\dot{W}_E$, represent the total respiratory, inspiratory, and expiratory work rate in kg·m/sec, respectively. Efficiency factors ξ_1 and ξ_2 account for the effects of respiratory-mechanical limitation and the decrease in neuro-mechanical efficiency with increasing effort.

2.2 The Waveshape of Neuromuscular Drive

The neuro-mechanical effector can be described by the electrical analog of modeled respiratory mechanics that describes the resistances and elastance of the lung, chest wall, and airways. The neuromuscular driving pressure waveform (P(t), cm-H_2O) is modeled as inspiratory and expiratory phases. The inspiratory pressure is approximated by a quadratic function, and the expiratory pressure is represented by an exponential discharge function of the form

$$P(t) = a_0 + a_0 t + a_0 t^2 \qquad 0 \le t \le t_1 \tag{5}$$

$$P(t) = P(t_1) \cdot e^{\frac{t-t_1}{\tau}} \qquad t_1 \le t \le t_1 + t_2 \ . \tag{6}$$

where the parameters a_0 and a_1 in Eq. (5) represent, respectively, the net driving pressure and its rate of increase at the onset of the neural inspiratory phase respectively, and the parameter a_2 describes the shape of the wave; τ denotes the declining rate of inspiratory activity, t_1 (sec) and t_2 (sec) represent the neural inspiratory and expiratory durations, respectively. In Eq. (6), $P(t_1)$ is the peak inspiratory pressure (in cm-H_2O) at the end of inspiration (t_1), and τ denotes the rate of decline of inspiratory activity. We previously have successfully simulated the optimized neuromuscular drive [7-9] with linear breathing mechanics of an RC model under eucapnia and hypercapnia at various levels of exercise CO_2 output and inhaled CO_2.

2.3 The Gas Exchanger

The plant of Gas Exchanger in Fig. 1 describes the events of the pulmonary exchange subject to the control signal $\dot{V}_E$ (total ventilation, l/min), disturbances in the inhaled and metabolic CO_2 (P_{ICO_2}, Torr, $\dot{V}_{CO_2}$, l/min). The system's output is the pressures of arterial CO_2 (P_{aCO_2}, Torr). The gas exchanger equation describes the dependence of P_{aCO_2} on the total ventilation and other disturbances:

$$P_{aCO_2} = P_{ICO_2} + \frac{863 \cdot \dot{V}_{CO_2}}{\dot{V}_A} = P_{ICO_2} + \frac{863 \cdot \dot{V}_{CO_2}}{\dot{V}_E\left(1 - \frac{V_D}{V_T}\right)} \ . \tag{7}$$

where P_{aCO_2} is assumed to be identical to the mean alveolar P_{CO_2}. Equation (8) describes the steady-state effect of ventilation on P_{aCO_2} subject to any disturbances in the inhaled and metabolic production of CO_2. To account for the changes in anatomic dead space with an airway caliber, the empirical relation [22] of Eq. (8) is employed:

$$V_D = 0.037 \cdot VC \cdot \left(1 + \frac{V_T}{8}\right) . \tag{8}$$

where VC is the vital capacity (l) and V_T is the tidal volume (l), EDS is the imposed external dead space (l). In current study, it was aimed to examine the comparison of linear and nonlinear respiratory mechanics on the model behavior of the optimal respiratory control, the external dead space was set to be nil. Based on the optimized pressure profile of Eqs. (5) and (6), for any given respiratory resistance and elastance, the breathing patterns, including tidal volume (V_T, l), breathing frequency (f, bpm), total ventilation ($\dot{V}_E$, l/min), and alveolar ventilation ($\dot{V}_A$, l/min) can be obtained.

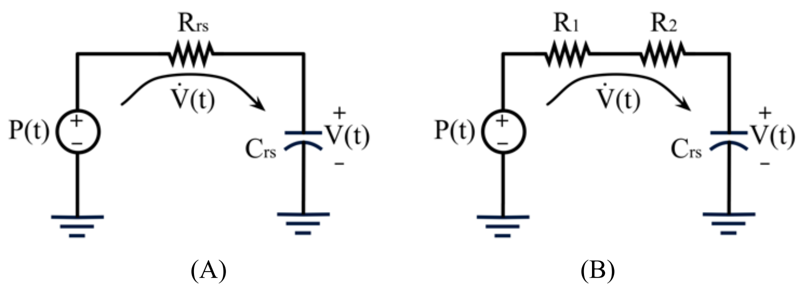

Figure 2. The electric RC model of the neuro-mechanical effector with (A) linear respiratory mechanics, and (B) nonlinear respiratory mechanics.

2.4 The Neuro-mechanical Effector

Linear Respiratory Mechanics. Such effector was described by the electrical R-C model of Fig. 2(A) based on a lumped-parameter model [13,14] for the relation between respiratory neural and mechanical outputs. In this model, the equation of motion is given by the following dynamic equation:

$$P(t) = \dot{V}(t) \cdot R_{rs} + V(t) \cdot E_{rs} \, . \tag{9}$$

The parameters R_{rs} (cm-$H_2O \cdot l^{-1} \cdot s$) and E_{rs} (=1/C_{rs}, cm-$H_2O \cdot l^{-1}$) in Eq. (9) represent the total flow-resistive and volume-elastic components, respectively. These include the passive resistances and elastance of the lung, chest wall, and airways. Thus the nonlinear pressure-flow and pressure-volume characteristics are linearized about the relaxation pressure.

Nonlinear Respiratory Mechanics

We employed the nonlinear respiratory mechanics that were expressed by time invariant resistive and elastic component. The system was also expressed using the simplest serial RC circuit, but the R_{rs} in Eq. (9) is replaced by R_1 and R_2 [5], as illustrated in Fig. 2(B). The driving pressure P(t) for the respiratory system was expressed as

$$\begin{aligned} P(t) &= \dot{V}(t) \cdot R_1 + \dot{V}(t)^2 \cdot R_2 + V(t) \cdot E_{rs} \\ &= \dot{V}(t) \cdot \left(R_1 + \dot{V}(t) \cdot R_2\right) + V(t) \cdot E_{rs} \end{aligned} \, . \tag{10}$$

where E_{rs} again is the lumped elastance of the total respiratory system, including the bronchi to alveoli and thorax. R_l is the lumped viscous resistance of the flow through the total respiratory system and R_2 is the second kind resistance of the flow that is proportional to the power of the rate of flow. Indeed, to be compared with the linear mechanics model of Eq. (9), the equivalent R_{rs} of Eq. (10) can be expressed as

$$R_{rs(eq)} = R_1 + \dot{V}(t) \cdot R_2 \, . \tag{11}$$

The model of the optimal chemical-mechanical respiratory control and simulation prospect of current study are illustrated in Fig. 1.

3 Result and Discussions

In the resting state, P_{ICO_2} is set to be 0% and $\dot{V}_{CO_2}$ is set to be 0.2 (l/min). The eucapnic responses were simulated by setting CO_2 inhalation to P_{ICO_2}=1~7%. The system response to moderate muscular exercise can be achieved varying $\dot{V}_{CO_2}$ within the range of 0.2~1.0 l/min. In our previous study with linear respiratory mechanics on the optimal respiratory control model [7-11], the parameters for airway resistance and elastance were set at R_{rs} = 3.02 (cm-$H_2O \cdot l^{-1} \cdot s$) and E_{rs} = 21.9 (cm-$H_2O \cdot l^{-1}$) for normal load, respectively.

The simulations results demonstrate that the linear respiratory mechanics model optimized the inspiratory phase of neuromuscular drive (P(t)) with a more convex upward shape under increased level of CO_2 inhalation (Fig. 3), and with a ramp-like shape of increasing rate under increased exercise input (Fig. 4). The nonlinear respiratory mechanics model optimized the inspiratory phase of P(t) with same ramp-like fashion in both CO_2 inhalation and exercise simulations, but attained higher amplitudes and steeper rising rates compared with the linear model. The airflow profile during the inspiratory phase, predicted using the linear model, was rectangular and exhibited a nearly constant flow rate during exercise (increased $\dot{V}_{CO_2}$), but became more peaked and convex and then decelerated toward the end of inspiration during CO_2 inhalation. By comparison with the nonlinear model, the airflow maintained a constant flow rate in the resting state but with a triangular profile in both the inspiratory and expiratory phases during exercise and CO_2 inhalation. The lung-volume profile obtained with the linear model retained a similar ramp-like behavior as the neuromuscular drive but with a higher peak (larger V_T) and a shorter duration (smaller T) during exercise and CO_2 inhalation. However, the nonlinear model achieved similar concave lung-volume waveshapes in both cases.

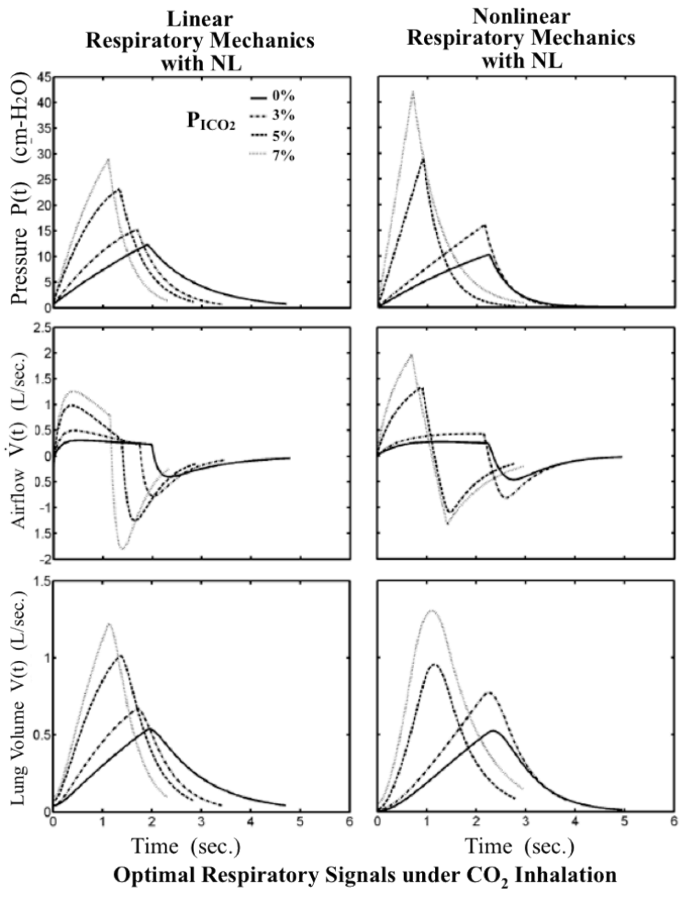

Figure 3. The optimal neuromuscular driving pressure (P(t), top), airflow ($\dot{V}(t)$, middle), and lung volume (V(t), bottom) with linear (left) and nonlinear (right) respiratory mechanics under CO_2 inhalation

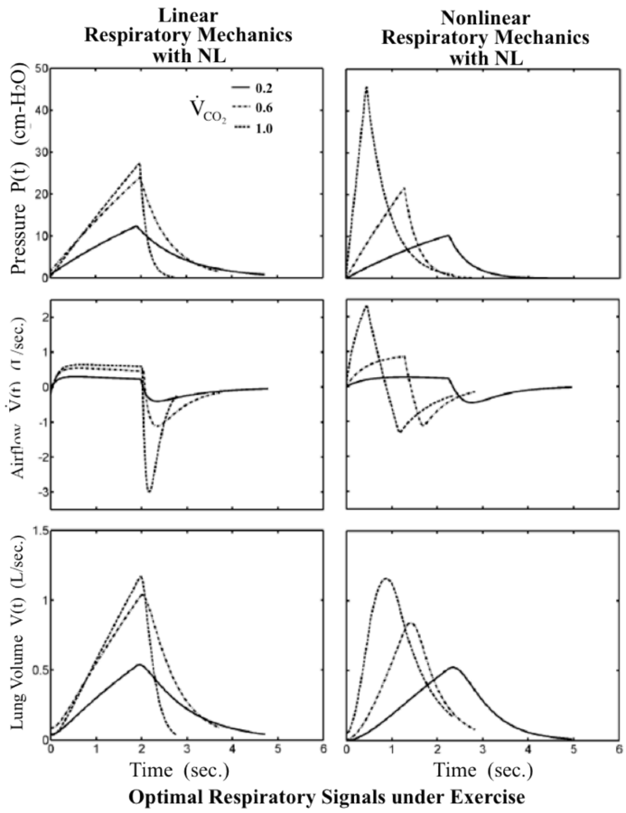

Figure 4. The optimal neuromuscular driving pressure (P(t), top), airflow ($\dot{V}(t)$, middle), and lung volume (V(t), bottom) with linear (left) and nonlinear (right) respiratory mechanics under exercise inputs

We compared 4 well-recognized ventilatory responses, based on linear and nonlinear respiratory mechanics with increased CO_2 and exercise input (Fig. 5). In both models, $\dot{V}_E$- P_{aCO_2} (Fig. 5, upper left) agreed with the hypothesized respiratory responses in which P_{aCO_2} remains constant during exercise input and rises linearly with increased ventilation during CO_2 inhalation. The hypercapnic response of the linear model was more sensitive to CO_2 (the slope of $\Delta\dot{V}_E/\Delta P_{aCO_2}$) than that of the nonlinear model. The relationships of $\dot{V}_E$-F (Fig. 5, upper right) for both models were similarly linear within the range where the relationship was linear. Under a fixed level of ventilation, the nonlinear model appeared to show higher breathing frequency during CO_2 inhalation and lower frequency during exercise in comparison with those in the linear model. The $\dot{V}_E$-V_T relationships (Fig. 5, lower left) were approximately linear in both models but with slightly differing slopes. As in the case of $\dot{V}_E$-F, the $\dot{V}_E$-V_T relationship in the linear model showed a larger gap between the eucapnic and hypercapnic simulations than the relationships in the nonlinear model. These results support the conclusion that the nonlinear model, unlike the linear model, acquires the intended level of ventilation with higher V_T and lower F during CO_2 inhalation and lower V_T

and higher F during exercise. Pervious experimental studies [23, 24] have shown that the duty cycle tends to vary between 0.4 and 0.6 over the range of ventilation and tidal volume level. In the relationships of $\dot{V}_E - T_I/T$ (Fig. 5, lower right), the duty cycle of the linear model climbed from a resting value of 0.52 to a maximum of 0.73 at the highest ventilation level. However, the nonlinear model predicted the duty cycle to range from 0.45 to 0.65 at a low ventilatory level ($\leq$ 10 L/min) and then to diminish to a minimum of approximately 0.2 at higher $\dot{V}_E$ (approximately 25 L/min).

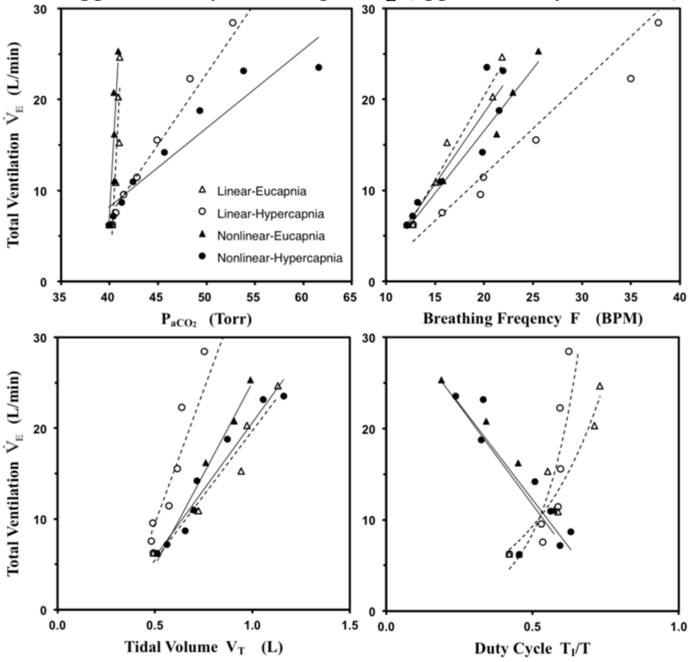

Figure 5. Predicted total ventilation $\dot{V}_E$ vs. arterial CO_2 pressure P_{aCO_2} (upper left), breathing frequency F (upper right), tidal volume V_T (lower left), and duty cycle T_I/T (lower right) during CO_2 inhalation (P_{ICO_2} = 0, 2~7%, ●○) and exercise ($\dot{V}_{CO_2}$ = 0.2~1.0, ▲△) with linear (○△) and nonlinear (●▲) respiratory mechanics model.

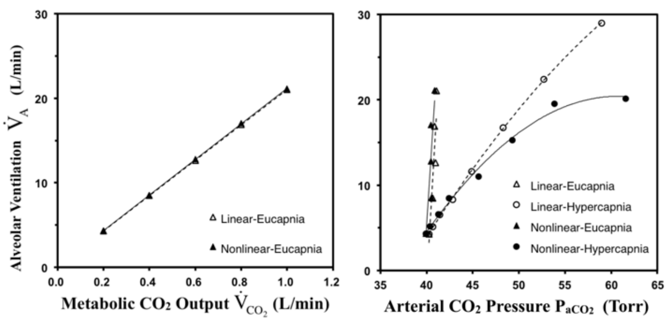

Figure 6. Predicted alveolar ventilation $\dot{V}_A$ versus metabolic CO_2 output $\dot{V}_{CO_2}$ (=0.2~1.0 L/min.) during eucapnia (left), and versus arterial CO_2 pressure P_{aCO_2} (right) during eucapnia (▲△) and hypercapnia (●○) with linear (○△) and nonlinear (●▲) respiratory mechanics model.

In Fig. 6 illustrates the predicted responses of alveolar ventilation ($\dot{V}_A$) of the two models to $\dot{V}_{CO_2}$(=0.2~1.0 L/min.) (Fig. 6, left) and to the resultant arterial CO_2 Pressure (P_{aCO_2}) (Fig. 6, right) under during eucapnia and hypercapnia. Notably, the $\dot{V}_A - \dot{V}_{CO_2}$ relationships were similar in the two models (Fig. 6, left). Whereas the relationship of $\dot{V}_A - P_{aCO_2}$ (triangles; Fig. 6, right) in the 2 models varied little during eucapnia, the $\dot{V}_A$ attained by the nonlinear model appeared to diminish exponentially at higher levels of hypercapnia ($P_{ICO_2} \geq 4\%$). Progressive hypercapnia at higher levels of $\dot{V}_A$ was also identified in an experimental sample [25], supporting the conclusion that P_{aCO_2} varies inversely (Eq. 7) with the $\dot{V}_A/\dot{V}_{CO_2}$ relationship.

4 Conclusion

In the study of the modelling of human respiratory control, the respiratory mechanics was often modelled as a lumped parameter R-C circuit for simulation simplification. In current study, we utilized the nonlinear system employed by Hirayama et al. [5], in which the respiratory mechanics are represented by a lumped elastance of the volume, a viscous resistance of the flow through the total respiratory system, and a second kind resistance of the flow that is proportional to the power of the rate of flow. However, instead of using a sinusoidal inspiratory airflow in the optimization through a six-nonlinear-term criterion, we applied the nonlinear respiratory mechanics model in the optimal chemical-mechanical respiratory control model that is proposed and verified [7-11] to obtain the optimal instantaneous respiratory signals and breathing patterns. To evaluate the performance of the nonlinear mechanics with the optimal respiratory control model, the eucapnia and hypercapnia were simulated with exercise input and CO_2 inhalation. We demonstrated the optimal respiratory signals, including the neuromuscular driving pressure, airflow, and lung volume profile, and examined the resultant ventilatory responses with the optimized breathing patterns.

In compared with profiles in the linear model, the optimal instantaneous profile of P(t) and V(t) of nonlinear respiratory mechanics model resembled a ramp-like waveshapes with steeper rising rate (larger a_1) and higher peak amplitude (higher A and V_T) under both hypercapnic and eucapnic conditions. Instead of resembling an inspiratory rectangular waveform during exercise and a descending waveform during CO_2 inhalation that were attained with linear model, the nonlinear model showed triangular airflow waveshapes in both inspiratory and expiratory phases under eucapnia and hypercapnia. The inspiratory waveform in the nonlinear model was also unlike the sinusoidal shape obtained by the linear model and remained triangular. By comparing the well-recognized ventilatory responses of $\dot{V}_E$ vs. P_{aCO_2}, $\dot{V}_E$ vs. F, $\dot{V}_E$ vs. V_T, $\dot{V}_E$ vs. T_I/T, $\dot{V}_A$ vs. $\dot{V}_{CO_2}$, and $\dot{V}_A$ vs. P_{aCO_2}, we determined that the nonlinear model, unlike the linear model, attained the intended level of ventilation with higher V_T and lower F during CO_2 inhalation and lower V_T and higher F during exercise. The response of $\dot{V}_A$ vs. P_{aCO_2} with the nonlinear model agreed more strongly than the response with the linear model with the experimental sample, in which the alveolar ventilation level decreased exponentially with increasing levels of hypercapnia.

This study provides a framework for further exploiting the ventilatory control behavior of the nonlinear breathing mechanics to optimize respiratory signals and breathing patterns. To recognize the effect of using the nonlinear respiratory mechanics in the optimal respiratory control model developed previously, we used the original performance indices of Eqs. (1)–(4), which were shown to be effective in earlier studies using the linear mechanics model. The mechanical cost of breathing was generated mainly with the total inspiratory and expiratory work rates. Because a nonlinear resistance proportional to the flow rate (Eq. (11)) is used during optimization in the nonlinear mechanics model, the inclusion of extra nonlinear terms corresponding to the airflow ($\dot{V}(t)$) or volume acceleration ($\ddot{V}(t)$) may account for the potential cost of breathing expended in maintaining the peak flow rate or defending against lung rupture. In accordance with the work of Hirayama et al. [5], a cost function containing a set of linear and nonlinear terms could also be applied to the optimal respiratory control model in future study. However, the time required for computing the optimal solution grew tremendously because of the involvement of the nonlinear terms in the performance index and in the resultant fourth order Runge-Kutta approximation of $\dot{V}(t)$ in each functional evaluation of J.

Acknowledgment

This study was supported by the National Science Council, Taiwan, under grant NSC 100-2221-E-035 -007, 101-2221-E-035 -005, and 102-2221-E-035-038.

References

1. Yamashiro, S.M., Daubenspeck, J.A., Lauritsen, T.N., F.S. Grodins: Total work rate of breathing optimization in CO2 inhalation and exercise. J. Appl. Physiol. 38, 702-709 (1975)
2. Luijendijk, S.C.M., Milic-Emili, J.: Breathing patterns in anesthetized cats and the concept of minimum respiratory effort. J. Appl. Physiol. 64, 31-41 (1988)
3. Rybak, A., Pottmann, M., Ogunnaike, B.A., Schwaber, J.S.: A closed-loop model of the respiratory control system. In: Proc. of Am. Control Conf., Seattle, Washington, USA (1995)
4. Mitsis, G.D.: Nonlinear data-driven modeling of cerebrovascular and respiratory control mechanisms. In: Proc. of 9th International Conf. on Inform. Tech. and Appl. in Biomed., Larnaca, Cyprus (2009)
5. Hirayama, H., Shimizu Y., Fukuyama, Y.: Optimal control of nonlinear respiratory system with performance function involving nonlinear terms. In: Proc. of 34th SICE Annual Conf., pp. 1229-1234. July 26-28, Sapporo, (1995)
6. Poon, C.S.: Ventilatory control in hypercapnia and exercise, optimization hypothesis. J. Appl. Physiol. 62, 2447-2459 (1987)
7. Poon, C.S., Lin, S.L., Knudson, O.B.: Optimization character of inspiratory neural drive. J. Appl. Physiol. 72, 2005-2017 (1992)
8. Lin, S.L., Chiu, C.C.: Optimizing the neuro-mechanical drive for human respiratory system. J. Biomed. Eng. Appl. Basis Comm. 6, 95-103 (1994)
9. Lin, S.L., Guo, N.R., Chiu, C.C.: Modeling and simulation of respiratory control with LabVIEW. J. Med. Biol. Eng. 32(1), 51-60 (2012)

10. Lin, S.L., Guo, N.R., Chen, T.C.: Optimal Respiratory Control Simulation and Comparative Study of Hypercapnic Ventilatory Responses to External Dead Space Loading. J. Mech. Med. Biol. Oct. (2013)
11. Lin, S.L., Chen, T.C., Chang, H.C.: Optimization of the Neural Muscular Drive and Respiratory Signals under Dead Space Loading and CO_2 Inhalation. In: Proc. Int. Appl. Sci. and Prec. Eng. Conf. G1034, NanTou, Taiwan (2013)
12. Guyenet, P.G., Stornetta, R.L., Abbott, S.B.G., Depuy, S.D., Fortuna, M.G., Kanbar, R.: Central CO2 chemoreception and integrated neural mechanisms of cardiovascular and respiratory control. J. Appl. Physiol. 108, 995-1002 (2010)
13. Younes, M., Riddle, W.: A model for the relation between respiratory neural and mechanical outputs, I. Theory. J. Appl. Physiol. 51, 963-977 (1981)
14. Younes, M., Riddle, W.: A model for the relation between respiratory neural and mechanical outputs, II. Methods. J. Appl. Physiol. 51, 979-989 (1981)
15. Tehrani, F.T.: Optimal control of respiration in exercise. In Proc. Conf. IEEE Eng. Med. Biol. Soc., pp. 3211-3214, 20, (1998)
16. Macklem, P.T.: A Century of the Mechanics of Breathing," Am. J. Respir. Crit. Care Med. 170, 10-15 (2004)
17. Kuebler, W.M., Mertens, M., Pries, A.R.: A two-component simulation model to teach respiratory mechanics. Advan. in Physiol. Edu. 31(2), 218-222 (2007)
18. Anderson, J., Goplen, C., Murray, L., Seashore, K., Soundarrajan, M., Lokuta, A., Strang, K., Chesler, N.: Human respiratory mechanics demonstration model. Advan. in Physiol. Edu. 33(1), 53-59 (2009)
19. Held, H.E., Pendergast, D.R.: Relative effects of submersion and increased pressure on respiratory mechanics, work, and energy cost of breathing. J. Appl. Physiol. 114(5), 578-591 (2013)
20. Moriondo, A., Pelosi, P., Passi, A., Viola, M., Marcozzi, C., Severgnini, P., Ottani, V., Quaranta, M., Negrini, D.: Proteoglycan fragmentation and respiratory mechanics in mechanically ventilated healthy rats. J. Appl. Physiol. 103(3), 747-756 (2007)
21. Ora, J., Laveneziana, P., Wadell, K., Preston, M., Webb, K.A., O'Donnell, D.E.: Effect of obesity on respiratory mechanics during rest and exercise in COPD. J. Appl. Physiol. 111(1), 10-19 (2011)
22. De Troyer, A., Cappello, M., Leduc, D., Gevenois, P.A.: Role of the mediastinum in the mechanics of the canine diaphragm. J. Appl. Physiol. 109(1), 27-34 (2010)
23. Poon, C.S.: Effects of inspiratory elastic load on respiratory control in hypercapnia and exercise, J. Appl. Physiol. 66, 2400-2406 (1989)
24. Thompson W., Carvalho, P., Souza, J., Charan, N.: Effect of expiratory resistive loading on the noninvasive tension-time index in COPD. J. Appl. Physiol., 89, 2007-2014 (2000)
25. Phillipson, E., Bowes, G., Townsend, E., Duffin, J., Cooper, J.: Role of metabolic CO2 production in ventilatory response to steady-state exercise, J. Clin. Invest. 68: 768–774 (1981)